



RESEARCH ARTICLE

10.1002/2017JD027477

Key Points:

- The simulations more reasonably estimate interannual variations than the climatology in soil temperature and active layer thickness
- The CFSR- and ERA-I-based simulations overall give more reasonable results than the MERRA-based simulation
- Different atmospheric forcing data sets result in a range of -5.8% to -9.0% for the change in permafrost area and a range of 9.9% – 20.2% for the change in active layer thickness

Correspondence to:

D. Guo,
guodl@mail.iap.ac.cn

Citation:

Guo, D., Wang, H., & Wang, A. (2017). Sensitivity of historical simulation of the permafrost to different atmospheric forcing data sets from 1979 to 2009. *Journal of Geophysical Research: Atmospheres*, 122. <https://doi.org/10.1002/2017JD027477>

Received 18 JUL 2017

Accepted 4 NOV 2017

Accepted article online 8 NOV 2017

Sensitivity of Historical Simulation of the Permafrost to Different Atmospheric Forcing Data Sets from 1979 to 2009

Donglin Guo^{1,2,3} , Huijun Wang^{2,1}, and Aihui Wang¹

¹Nansen-Zhu International Research Center, Institute of Atmospheric Physics, Chinese Academy of Sciences, Beijing, China,

²Key Laboratory of Meteorological Disaster, Ministry of Education/Collaborative Innovation Center on Forecast and Evaluation of Meteorological Disasters, Nanjing University of Information Science and Technology, Nanjing, China, ³Joint Laboratory for Climate and Environmental Change, Chengdu University of Information Technology, Chengdu, China

Abstract Numerical simulation is of great importance to the investigation of changes in frozen ground on large spatial and long temporal scales. Previous studies have focused on the impacts of improvements in the model for the simulation of frozen ground. Here the sensitivities of permafrost simulation to different atmospheric forcing data sets are examined using the Community Land Model, version 4.5 (CLM4.5), in combination with three sets of newly developed and reanalysis-based atmospheric forcing data sets (NOAA Climate Forecast System Reanalysis (CFSR), European Centre for Medium-Range Weather Forecasts Re-Analysis Interim (ERA-I), and NASA Modern Era Retrospective-Analysis for Research and Applications (MERRA)). All three simulations were run from 1979 to 2009 at a resolution of $0.5^\circ \times 0.5^\circ$ and validated with what is considered to be the best available permafrost observations (soil temperature, active layer thickness, and permafrost extent). Results show that the use of reanalysis-based atmospheric forcing data set reproduces the variations in soil temperature and active layer thickness but produces evident biases in their climatologies. Overall, the simulations based on the CFSR and ERA-I data sets give more reasonable results than the simulation based on the MERRA data set, particularly for the present-day permafrost extent and the change in active layer thickness. The three simulations produce ranges for the present-day climatology (permafrost area: $11.31\text{--}13.57 \times 10^6 \text{ km}^2$; active layer thickness: 1.10–1.26 m) and for recent changes (permafrost area: -5.8% to -9.0% ; active layer thickness: 9.9% – 20.2%). The differences in air temperature increase, snow depth, and permafrost thermal conditions in these simulations contribute to the differences in simulated results.

1. Introduction

Simulation is of great importance for the study of frozen-ground change on regional and long-term temporal scales. Frozen ground includes permafrost and seasonally frozen ground (Muller, 1947), with the former covering approximately 25% of the land area in the Northern Hemisphere (Zhang et al., 1999). Studies have shown that severe permafrost degradation can significantly affect hydrology and water resources (Cuo et al., 2015; Liljedahl et al., 2016; Yang et al., 2014), ecosystems (Qin et al., 2014; Yang et al., 2010; Yi et al., 2014), human engineering facilities (Guo & Sun, 2015; Guo & Wang, 2016a; Nelson et al., 2002), and climate change (Schuur et al., 2015). These impacts have made permafrost change a hot topic in climate change research in the context of the recent and the projected future climate warming (Collins et al., 2013). Permafrost is mostly distributed in high-latitude and high-elevation regions. Observations are scarce and are of a short-term nature in these regions because the cold climate and often rugged topography make conventional ground measurements difficult. The study of permafrost dynamics on large spatial and long-term temporal scales by ground observations is therefore limited. Thus, there is a need for a numerical simulation method that can be used to study permafrost change and its associated mechanisms on regional and long-term temporal scales.

Simulations of frozen ground have largely been advanced by a series of improvements in frozen-ground-related processes in models (Lawrence et al., 2008, 2012). Using version 3.0 of the Community Climate System Model, with the CLM3.0 (Community Land Model, version 3.0) land module, Lawrence and Slater (2005) projected a severe near-surface permafrost degradation of 60–90% by 2100. Burn and Nelson (2006) argued that such a severe degradation is not likely to occur and that the results may be

1
2
3
4
5
6
7
8
9
10
11
12
13
14
15
16
17
18
19
20
21
22
23
24
25
26
27
28
29
30
31
32
33
34
35
36
37
38
39
40
41
42
43
44
45
46
47
48
49
50
51
52
53
54
55
56
57
58
59
60
61
62
63
64
65
66

Q2 Q3

Q4

Table 1*Details of the Atmospheric Forcing Data Sets*

Variable	Resolution (°longitude × °latitude)	Mean annual air temperature (°C)	Annual maximum air temperature (°C)	Annual minimum air temperature (°C)	Mean annual soil temperature at 1 m depth (°C)	Winter snow depth (m)
CFSR	0.5° × 0.5°	−9.32 (0.44)	11.41 (0.30)	−28.62 (0.54)	−5.49 (0.46)	0.73 (0.01)
ERA-I	0.75° × 0.75°	−9.69 (0.50)	10.97 (0.30)	−30.52 (0.45)	−5.22 (0.60)	0.69 (0)
MERRA	0.5° × 0.33°	−9.47 (0.44)	12.16 (0.42)	−29.97 (0.39)	−4.19 (0.60)	0.64 (0.01)

Note. All variables are area-averaged values over observed permafrost region, with trends (per decade) from 1979 to 2009 shown in brackets.

overestimated, mostly due to the absence of the organic layer and shallow soil profile in the land model. Consequently, the organic layer of the surface was incorporated into the CLM4.0, and its impacts on frozen-ground simulation were examined by Nicolsky et al. (2007). In addition, the soil profile of the model has been significantly extended to account for the thermal inertia from the cold, deep permafrost layers (Alexeev et al., 2007; Lawrence et al., 2008). Furthermore, frozen-ground parameterizations and cold-region hydrology processes have also been corrected in the Community Land Model, version 4.5 (CLM4.5) (Niu & Yang, 2006; Swenson et al., 2012). These efforts have improved the performance of frozen-ground simulations from a model development perspective.

The performance of frozen-ground simulations is also affected by atmospheric forcing data set (Guo et al., 2012; Lawrence et al., 2012). For example, Guo et al. (2012) performed a correction to atmospheric forcing data set from a dynamical downscaling simulation in order to decrease the bias in the simulation of permafrost on the Tibetan Plateau. Lawrence et al. (2012) found that the projected rate of permafrost degradation reduced to approximately 29% after the simulated climate biases in air temperature and precipitation that were inputted into the land surface model were ameliorated.

In the present study, three sensitivity simulations were performed using the latest version of CLM4.5, driven respectively by different atmospheric forcing data sets, to address the issue as to what extent the variation in the atmospheric forcing data set affects the simulated permafrost conditions and changes. Three reanalysis-based atmospheric forcing data sets were newly developed before the simulation was performed. In addition, comprehensive frozen-ground observations, including soil temperature, active layer thickness, and permafrost extent, were collected to validate the simulated results.

2. Data, Model, Experimental Design, and Methods

2.1. Data

The three reanalysis data sets used to develop an atmospheric forcing data set were the National Oceanic and Atmospheric Administration Climate Forecast System Reanalysis (CFSR) (Saha et al., 2010), the European Centre for Medium-Range Weather Forecasts Re-Analysis Interim (ERA-I) (Dee et al., 2011), and the National Aeronautics and Space Administration Modern Era Retrospective-Analysis for Research and Applications (MERRA) (Rienecker et al., 2011). The original horizontal (and temporal) resolutions are 0.5° × 0.5° (6-hourly), 0.75° × 0.75° (3-hourly), and 0.5° × 0.33° (hourly) for CFSR, ERA-I, and MERRA, respectively (Table 1). All these reanalysis data sets start at 1979 and have been continually updated to the present day. These reanalysis data sets have been confirmed to be more accurate than the earlier ones, such as the National Centers for Environmental Prediction-National Center for Atmospheric Research reanalysis (Rienecker et al., 2011), and have been widely used to assess past climate conditions and to drive numerical models (Chen et al., 2017; Fan et al., 2016; Gao et al., 2016; Sun, 2017; Wang & Zeng, 2012; Zhou et al., 2016).

Soil temperature observations at depths of 1 m and 6 m were obtained from Russian meteorological station (RMS) (<http://meteo.ru/english/climate/soil.php>) and International Polar Year thermal state of permafrost (IPY-TSP) (Romanovsky et al., 2010) data (<http://nsidc.org/data/G02190>), respectively. The RMS data were measured at depths ranging from 0.02 to 3.2 m. They cover the total period from 1963 to 2011 but are not continuous, and many stations have shorter observation periods than this. Only the data for the period 1981–2009 were used in this study to validate the simulated results, because most stations have continuous records during this period. These data are reliable because a strict quality control procedure was carried out in the postprocessing stage of the data. The IPY-TSP data were measured at depths ranging from 0 to 100 m.

They cover a total period from 2006 to 2010, but this is not the case for all stations. The IPY-TSP data are also reliable and have been used to validate published model results (Guo & Wang, 2016a; Lawrence et al., 2012). For both RMS and IPY-TSP data, soil temperature at the depths of interest (1 m and 6 m) were not measured directly but were calculated by simple linear interpolation between known values, which is allowed due to the linear relationship of mean soil temperature with depth (Koven et al., 2013).

Active layer thickness observations were obtained from two sources: (1) the Circumpolar Active Layer Monitoring (CALM) network (Brown et al., 2000) (<http://www.gwu.edu/~calm/>); and (2) the historical active layer thickness estimated from the observed soil temperatures at 31 weather stations in Russia (AL_RHST) (Zhang et al., 2006) (<https://data.eol.ucar.edu/dataset/106.ARCSS160>). The CALM data cover the period from 1990 to 2015, although measurements at many stations are not continuous and begin in 1996. The data for the period 1996–2007 were used in this study because most of the stations have continuous records during this period. The AL_RHST data cover the period 1930–1990, and the data for 1981–1990 were used in this study for validating the model results during the corresponding period. These two sets of active layer thickness data are reliable and have been employed to validate the results of climate models (Guo & Wang, 2016a; Lawrence et al., 2012). Notably, for the validation of present-day climatology, site observations were first averaged over the periods that have records at each station and then compared to the corresponding grid mean simulated values. For the validation of interannual variation, station observations were first averaged over all stations and then compared to the corresponding grid mean simulated results.

Permafrost extent observations, used to validate the simulated present-day permafrost distribution, were obtained from the circum-Arctic map of permafrost and ground ice conditions (Brown et al., 1997). The data have a resolution of $0.5^\circ \times 0.5^\circ$ and are available at http://nsidc.org/data/docs/fgdc/ggd318_map_circumarctic/index.html. These data are considered to be the best available for permafrost. In this data set, permafrost is classified into continuous, discontinuous, isolated, and sporadic, but it is argued that only continuous and discontinuous permafrost could be captured by climate models due to their coarse horizontal resolution (Burn & Nelson, 2006). We therefore only compared these two types to the simulated results. It should be noted that this would not be appropriate if higher-resolution simulation were performed.

2.2. Model

The latest version of CLM (CLM4.5), was used in this study. CLM4.5 is an update of CLM4.0 (Oleson et al., 2013). CLM has undergone a series of improvements since version 3.0 (Lawrence et al., 2011). These include a revision of the surface data sets (Lawrence & Chase, 2007), the incorporation of a two-leaf model for photosynthesis (Thornton & Zimmermann, 2007), modifications to the snow model (Flanner et al., 2007; Wang & Zeng, 2009), inclusion of a TOPMODEL-based model for runoff (Niu et al., 2007), incorporation of a carbon-nitrogen biogeochemical model (Thornton et al., 2009; Wang et al., 2015; Xie et al., 2016), and corrections to the parameterization of frozen ground (Lawrence et al., 2011). The improvements with regard to frozen-ground simulation are incorporation of a freezing point depression expression for updating the freezing and melting processes (Niu & Yang, 2006), representation of the thermal and hydraulic properties of soil organic matter for reducing soil temperature (Nicolsky et al., 2007), deepening of the soil column to account for the thermal inertia resulting from the cold deep permafrost (Alexeev et al., 2007), and improvement to the hydrological processes in the cold region for moderating dry surface organic soil (Swenson et al., 2012). The performance of CLM in simulating frozen ground has been greatly improved by these upgrades (Koven et al., 2013; Lawrence et al., 2008), and it has been widely used to assess the historic and future dynamics of permafrost (Guo & Wang, 2013; Guo et al., 2012; Lawrence et al., 2012; Liu & Jiang, 2016).

2.3. Experimental Design

Three simulations were performed using CLM4.5, driven by three atmospheric forcing data sets (CFSR, ERA-I, and MERRA). The atmospheric variables required as input data by CLM4.5 include air temperature, precipitation, air pressure, wind speed, specific humidity, and downward short-wave radiation. All three simulations were conducted on a global scale, with a simulation period from 1979 to 2009. Spatial and temporal resolutions for the output of the simulations were set at $0.5^\circ \times 0.5^\circ$ and daily, respectively. For model initialization, the model was first run for 100 years, cyclically driven by CRUNCEP forcing data set (the default forcing data set in CLM4.5) from 1979, and the final states were saved. Using such final states as initial fields, the model was then run for 30, 30, and 40 years with the CFSR, ERA-I, and MERRA forcing data set from 1979,

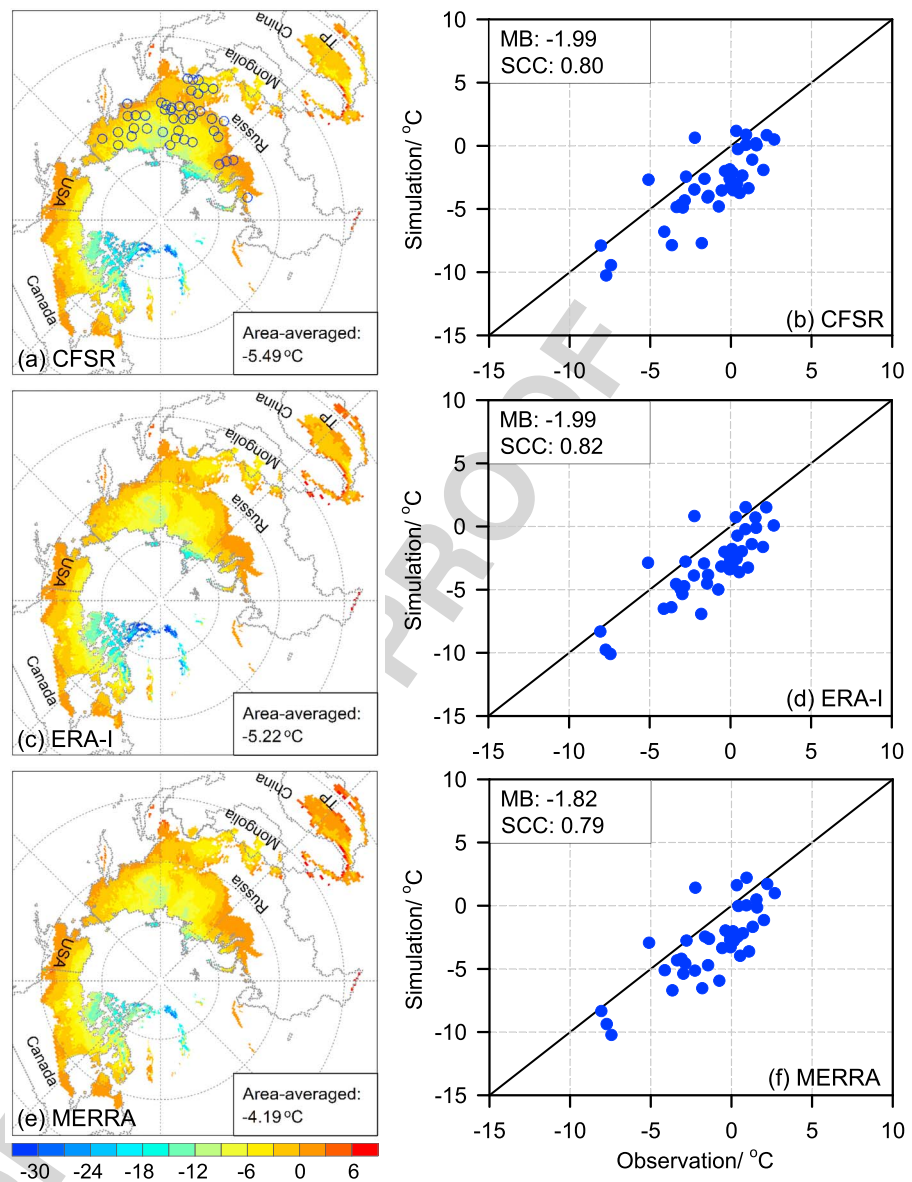


Figure 1. Simulated mean soil temperature (1981–2000) (°C) at a depth of 1 m over observed permafrost region based on the atmospheric forcing data set from (a) CFSR, (c) ERA-I, and (e) MERRA and (b, d, f) their validations with station observations during the corresponding period. Observation stations for the soil temperature are denoted with circles in Figure 1a. Area-averaged values are given in the bottom right corner of Figures 1a, 1c, and 1e. Mean bias (MB) and the spatial correlation coefficient (SCC) are given in the top left corner of Figures 1b, 1d, and 1f. All SCCs exceeded a significance level of 95%. Five countries and the Tibetan Plateau (TP), containing mostly permafrost, are outlined by the gray dashed lines.

respectively. At the end of these three initializations, the interannual variations in soil temperature were $<0.003^{\circ}\text{C}$ at 0–7.8 m (the analyzed deepest depth) soil levels, which could be regarded as the model arriving at the equilibrium states. For each initialization run, the final states were saved and used to initiate the corresponding transient simulation from 1979 to 2009.

2.4. Methods

Three new atmospheric forcing data sets (CFSR, ERA-I, and MERRA) were developed based on the original reanalysis data sets. The three original reanalysis data sets were interpolated into a common horizontal resolution of $0.5^{\circ} \times 0.5^{\circ}$ but retaining the original temporal resolution. A bilinear interpolation method was

employed to downscale the meteorological variables of air temperature, pressure, wind, specific humidity, and downward short-wave radiation. For precipitation, the bilinear interpolation method would reduce the spatial variability and produce incorrect results due to the temporal heterogeneity of precipitation. The following method was therefore used in this study: The original grid box of reanalysis precipitation was first divided into $0.01^\circ \times 0.01^\circ$ pixels, with the amount of precipitation remaining unchanged. Then, the average of precipitation of the pixels within a common grid cell of $0.5^\circ \times 0.5^\circ$ was taken as the value of this common grid cell. With this method, the precipitation amount in a specified area remained the same before and after downscaling. More details of the development of these forcing data sets can be found in Wang et al. (2016).

Bias in the reanalysis precipitation was corrected during the development of the new atmospheric forcing data set. Previous studies have indicated that reanalysis precipitation data (e.g., CFSR, ERA-I, and MERRA) have large biases against observation-based precipitation products (Bosilovich et al., 2011). The monthly precipitation product from the Global Precipitation Climatology Project (GPCP), version 2.2 (Huffman et al., 2009), was used to correct the bias in the reanalysis precipitation in this study. GPCP precipitation was produced by merging station observations and satellite measurements at a horizontal resolution of $2.5^\circ \times 2.5^\circ$. The GPCP precipitation was first divided into grid cells of resolution $0.5^\circ \times 0.5^\circ$. The ratio of monthly GPCP to monthly reanalysis precipitation was then calculated for each grid cell. The reanalysis precipitation was finally corrected by multiplying by this ratio at each time step in the same month. More details regarding the correction of bias in the precipitation reanalysis data can be found in Wang et al. (2016).

Permafrost is identified as ground where monthly soil temperature is less than 0°C for 24 consecutive months in at least one layer of the upper 10 soil layers (3.8 m) (Lawrence et al., 2012). It should be mentioned that this definition of permafrost represents “near-surface permafrost.” Generally, near-surface permafrost is more sensitive to climate change than deep permafrost (Lawrence et al., 2008). Loss of near-surface permafrost at a location does not mean that deep permafrost is also lost at this location. Near-surface permafrost was selected for investigation in this study and in previous studies (e.g., Lawrence et al., 2012) due to its greater sensitivity to climate change. The active layer thickness is the maximum depth of thaw for permafrost over the course of a year and was calculated based on daily soil temperature data (Lawrence et al., 2008).

Mean bias, mean absolute bias, correlation coefficients, and Nash-Sutcliffe efficiency (NSE) (Nash & Sutcliffe, 1970) were used to evaluate the level of agreement between the simulated and observed results. NSE denotes the relative magnitude of the residual variance compared to the variance of observation, indicating how closely the plot of simulations and observations fits the 1:1 line. The NSE statistic ranges from $-\infty$ to 1, and the closer it is to 1 the more accurate is the simulated result. The least squares fitting method was used to calculate the trend as the slope of the linear regression, and the Student's *t* test was used to assess the statistical significance of the linear trend.

3. Results

3.1. Soil Temperature

The three simulations show a similar spatial distribution in soil temperature climatology at a depth of 1 m (Figure 1). The differences are mostly seen over the Tibetan Plateau, where the simulated soil temperatures based on MERRA data are the warmest, followed by those based on ERA-I data, while the simulated soil temperatures based on CFSR data are the coolest. The area-averaged soil temperatures are -5.49 , -5.22 , and -4.19°C over the observed permafrost region for the simulations based on CFSR, ERA-I, and MERRA, respectively. The observation-based validation shows that all three simulated soil temperatures agree well with observations but with a cold bias ranging from -1.82 to -1.99°C (Figure 1 and Table 2).

The three simulations also show a similar spatial distribution in soil temperature climatology at a depth of 6 m (Figure 2). Similar to the situation at 1 m depth, the differences in the spatial distribution among the three simulations are mainly over the Tibetan Plateau. The area-averaged soil temperatures are -5.64 , -5.39 , and -4.35°C over the observed permafrost region for simulations based on CFSR, ERA-I, and MERRA, respectively. The simulated soil temperatures at 6 m depth have somewhat weaker correlations with the observations, but smaller mean absolute bias and larger NSE, compared to the simulated soil temperature at 1 m depth (Table 2). The soil temperatures at 6 m depth from the CFSR-based simulation fit better with observations than those from the ERA-I-based simulation, followed by those from the MERRA-based simulation.

Table 2

Statistics of Similarities Between the Simulated and Observed Soil Temperature Climatology at Depths of 1 and 6 m, Soil Temperature Change at a Depth of 1 m, Active Layer Thickness Climatology Based on CALM and AL_RHST Data, and Active Layer Thickness Change Based On CALM Data

Index	Soil temperature (°C)			Active layer thickness (m)		
	Climatology (1 m, 1981–2000) CFSR, ERA-I, MERRA	Climatology (6 m, 2006–2010) CFSR, ERA-I, MERRA	Change (1 m, 1981–2009) CFSR, ERA-I, MERRA	Climatology CALM, 1991–2000) CFSR, ERA-I, MERRA	Climatology (AL_RHST, 1981–1990) CFSR, ERA-I, MERRA	Change (CALM, 1996–2007) CFSR, ERA-I, MERRA
Mean bias	-1.99, -1.99, -1.82	0.22, 0.80, 1.16		0.21, 0.33, 0.66	-0.33, -0.29, -0.11	
Mean absolute bias	2.31, 2.30, 2.24	1.78, 2.07, 2.21		0.52, 0.63, 0.89	0.50, 0.44, 0.52	
Correlation coefficient	0.80, 0.82, 0.79	0.74, 0.63, 0.65	0.89, 0.92, 0.91	0.69, 0.62, 0.51	0.18, 0.41, 0.12	0.62, 0.83, 0.75
Nash-Sutcliffe efficiency	0, 0.05, 0.05	0.49, 0.30, 0.26	0.41, 0.38, 0.38	0.42, 0.25, -0.34	-0.56, -0.20, -0.47	-0.64, 0.36, -3.99

Note. The three simulations are based on atmospheric forcing data sets from CFSR, ERA-I, and MERRA. Bold type denotes a statistical significance >95%.

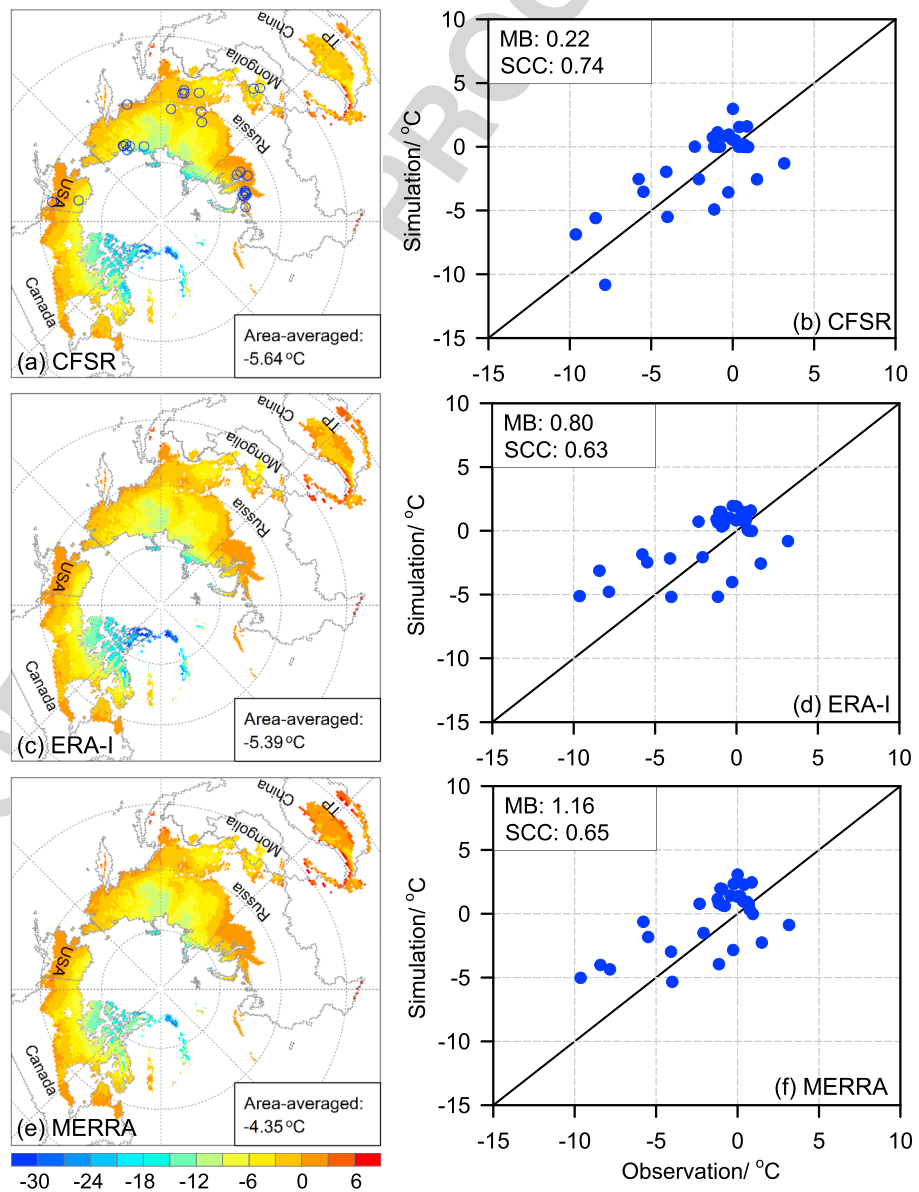


Figure 2. Same as in Figure 1 but for simulated mean soil temperature (1981–2000) (°C) at a depth of 6 m over (a, c, and e) observed permafrost region. In addition, the period for (b, d, and f) this validation is from 2006 to 2010, which is different from the period 1981–2000 for validation of soil temperature at a depth of 1 m in Figure 1.

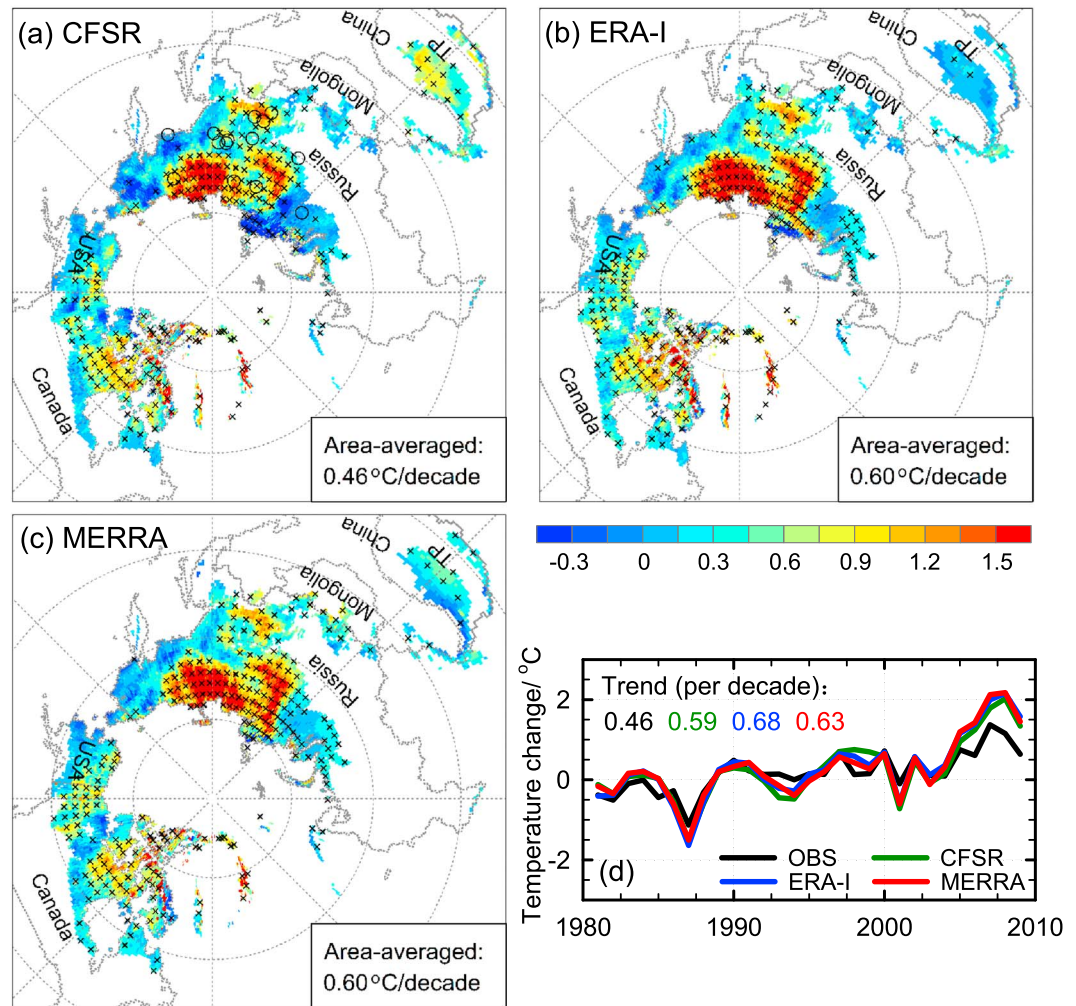


Figure 3. Distribution of trends in the simulated soil temperature ($^{\circ}\text{C decade}^{-1}$) at a depth of 1 m over observed permafrost region during the period 1979–2009 based on the atmospheric forcing data sets from (a) CFSR, (b) ERA-I, and (c) MERRA and (d) the validation of soil temperature change from 1981 to 2009 based on observations from Russian meteorological stations, denoted with black hollow circles in Figure 3a. Areas with significance levels exceeding 95% are denoted with crosses. Area-averaged values are given in the bottom right corner of Figures 3a–3c. The observed and simulated trends are given in the top left corner of Figure 3d. Five countries and the Tibetan Plateau (TP), containing mostly permafrost, are outlined by the gray dashed lines.

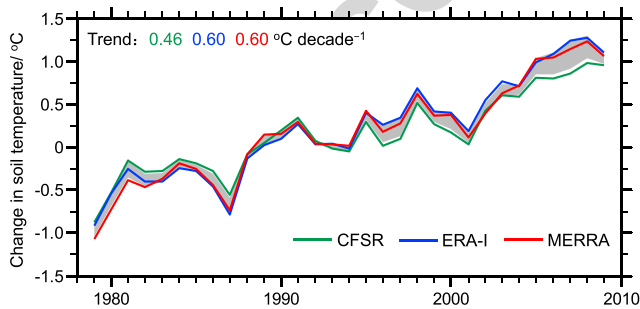


Figure 4. Simulated change in soil temperature ($^{\circ}\text{C}$) at a depth of 1 m from 1979 to 2009 based on atmospheric forcing data sets from CFSR, ERA-I, and MERRA, as averaged over observed permafrost region. Shaded areas represent one standard deviation across the simulations based on the three types of atmospheric forcing data sets. The simulated trends are given in the top left corner of the figure.

Similar spatial distributions of the trends of the simulated soil temperatures at 1 m depth are produced by the three simulations, except on the Tibetan Plateau where obvious differences in the trend are shown across the three simulations (Figure 3). The greatest increase in soil temperature is seen in Siberia, Russia, followed by the northern parts of Canada and Alaska. The area-averaged trends are 0.46, 0.60, and $0.60^{\circ}\text{C decade}^{-1}$ over the observed permafrost region for simulations based on CFSR, ERA-I, and MERRA, respectively. As shown in Figure 3d, the simulated variations in soil temperature agree well with observations, although the model overestimates the increase in soil temperature during the period 2006–2009. Compared to the trends in the soil temperature from the ERA-I-based simulation ($0.68^{\circ}\text{C decade}^{-1}$) and the MERRA-based simulation ($0.63^{\circ}\text{C decade}^{-1}$), the trend in the soil temperature from the CFSR-based simulation ($0.59^{\circ}\text{C decade}^{-1}$) is closer to the observed results ($0.46^{\circ}\text{C decade}^{-1}$).

Table 3

Present-Day Climatology (1981–2000), Trend in the Period 1979–2009, and Relative Change for Soil Temperature, Permafrost Area, and Active Layer Thickness

Variable	Present day (1981–2000)	Trend in 1979–2009 (per decade)	Relative change
Soil temperature (1 m) (°C)	-4.97 ± 0.56	0.55 ± 0.06	$29.4\% \pm 5.3\%$
Permafrost area ($\times 10^{12}$ km ²)	12.51 ± 0.93	-0.31 ± 0.03	$-7.1\% \pm 1.4\%$
Active layer thickness (m)	1.16 ± 0.07	0.05 ± 0.016	$15.4\% \pm 4.3\%$

Note. The range of uncertainty is one standard deviation across the simulations based on the three types of atmospheric forcing data sets. The relative change relative to 1979 is calculated as: $\text{trend} / 10 \times (2009 - 1979 + 1) / \text{value in 1979} \times 100\%$.

The three simulations give a consistently significant increase in area-averaged soil temperature during the period 1979–2009 (Figure 4). The trends are 0.46, 0.60, and 0.60°C decade⁻¹ for the simulations based on CFSR, ERA-I, and MERRA, respectively. The average trend is 0.55°C decade⁻¹, with one standard deviation of 0.06°C decade⁻¹ across the three simulations (Table 3). The relative change in soil temperature at 1 m depth is 22%, 30%, and 35% for the CFSR-, ERA-I-, and MERRA-based simulations, respectively.

3.2. Permafrost Area

The spatial distribution of present-day permafrost is captured by the three simulations, except for those over the Tibetan Plateau (Figure 5). The simulated permafrost extent is smaller than that from observations, especially for the ERA-I- and MERRA-based simulations. The model underestimates the permafrost extent in southern Alaska, the United States, in the northern Western Siberian Plain, Russia, and over the Tibetan Plateau. The simulated permafrost areas are 13.6×10^6 km², 12.6×10^6 km², and 11.3×10^6 km² for the simulations based on the CFSR, ERA-I, and MERRA data, respectively. These values are smaller compared to the observations being 15.2×10^6 km², due to the underestimation of permafrost extents in the three regions mentioned above. Among the three simulations, the permafrost extent from the CFSR-based simulation is the closest to observations, followed by the ERA-I- and MERRA-based simulations.

For the period 1979–2008, the decrease in permafrost extent mainly occurs at the southern edge of the permafrost, especially in Canada, eastern Russia, and the Tibetan Plateau (Figure 6). It can also be seen that the permafrost extent shows an increase in a small number of grids, which are mostly distributed at the southern edge of the permafrost in Alaska and the edge of permafrost in Sayan and on mountains in south Baikal. Overall, these spatial changes in permafrost extent are very similar for all three simulations.

The three simulations give a consistent decrease in permafrost area from 1979 to 2008 (Figure 6d). The decrease is especially distinct during the recent decade. The decreasing trends are 0.36, 0.28, and 0.29×10^6 km² decade⁻¹ for the CFSR-, ERA-I-, and MERRA-based simulations, respectively. The average trend

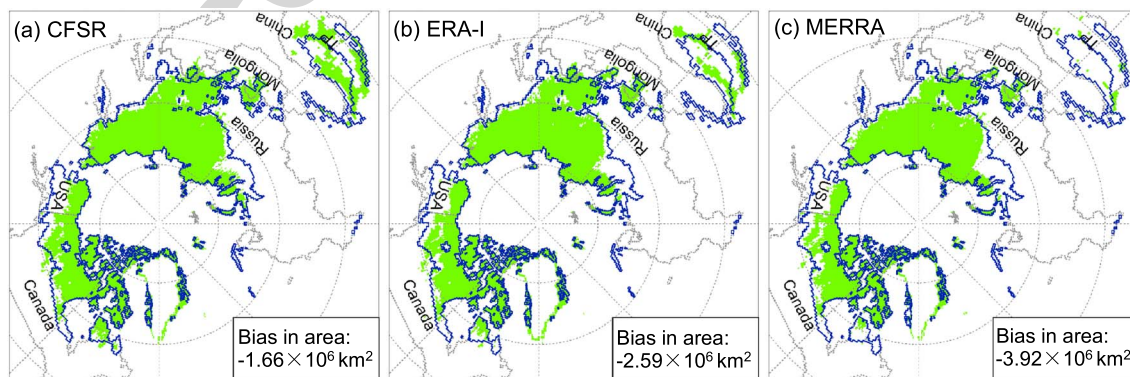


Figure 5. Comparison of the simulated present-day permafrost extent (shaded color) based on the atmospheric forcing data sets from (a) CFSR, (b) ERA-I, and (c) MERRA to observations (areas outlined in blue). The bias between the simulated and observed permafrost area is given in the bottom right corner of Figures 5a–5c. Five countries and the Tibetan Plateau (TP), containing mostly permafrost, are outlined by the gray dashed lines.

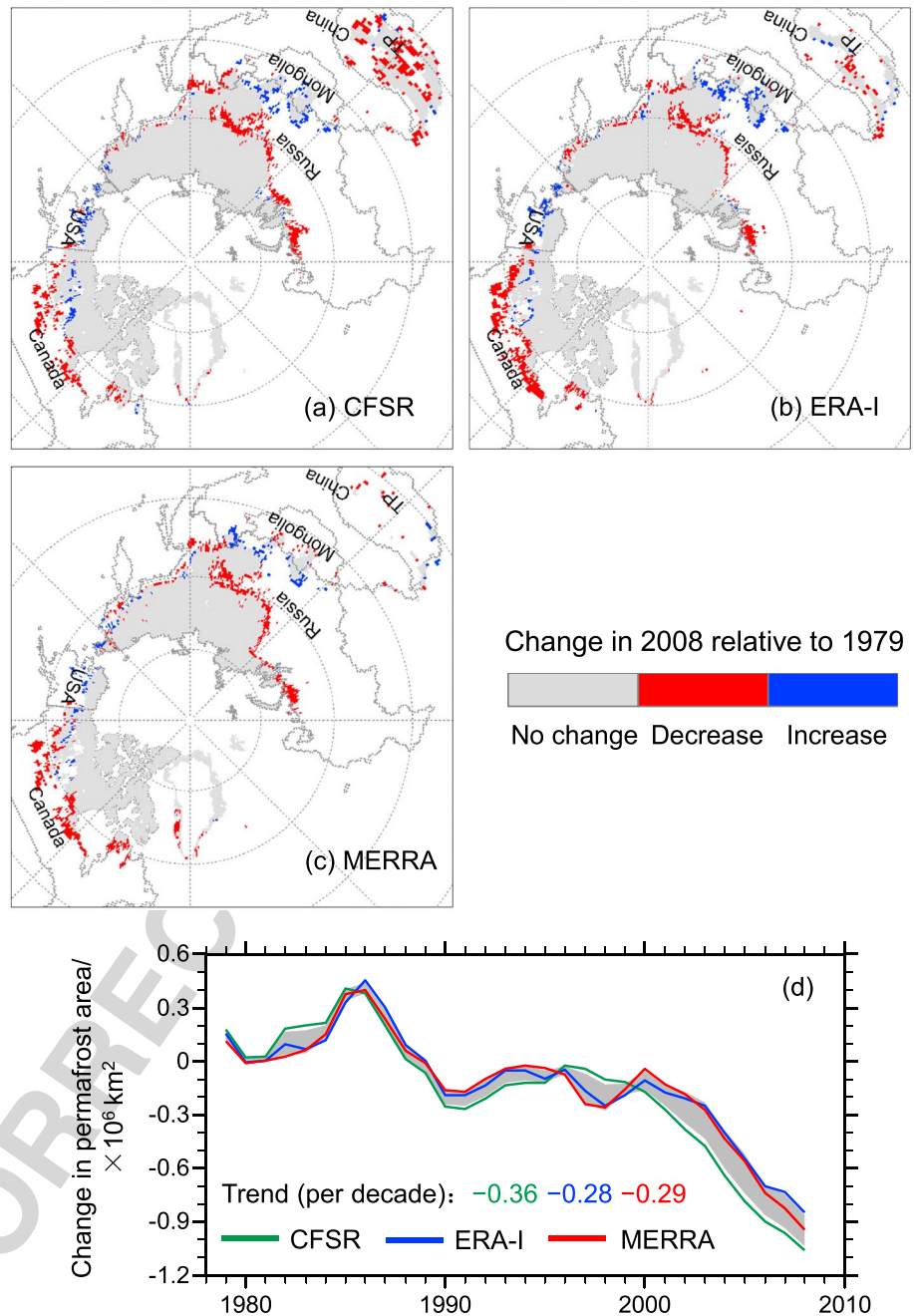


Figure 6. Spatial change in permafrost extent in 2008 relative to 1979 from the simulations based on the atmospheric forcing data sets from (a) CFSR, (b) ERA-I, and (c) MERRA and (d) the simulated change in permafrost area (10^6 km^2) from 1979 to 2009 based on atmospheric forcing data sets from CFSR, ERA-I, and MERRA. Five countries and the Tibetan Plateau (TP), containing mostly permafrost, are outlined by the gray dashed lines in Figures 6a–6c. Shaded areas in Figure 6d represent one standard deviation across the simulations based on the three types of atmospheric forcing data sets. The simulated trends are given in the bottom left corner of Figure 6d.

(Table 3). The relative change in the permafrost area is 5.8%, 6.5%, and 9.0% for the CFSR-, ERA-I-, and MERRA-based simulations, respectively.

3.3. Active Layer Thickness

The three simulations give a very similar spatial pattern for the active layer thickness climatology, (i.e., the active layer thickness decreases with increasing latitude; Figure 7). The active layer thickness ranges from 0

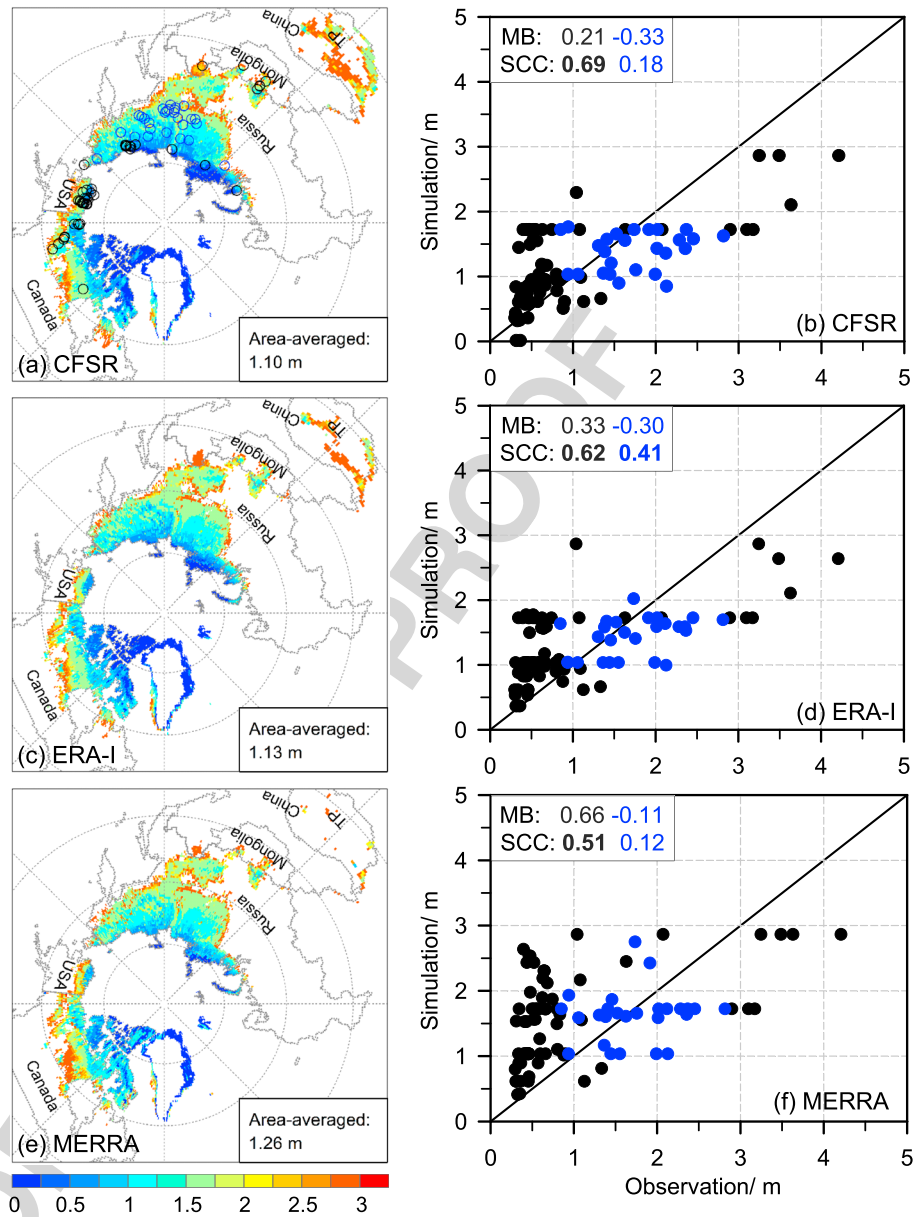


Figure 7. Same as in Figure 1 but for (a, c, and e) simulated mean active layer thickness (1981–2000) (m) over the present-day (1981–2000) simulated permafrost region. In addition, black (blue) solid circles represent the validation based on observations from CALM (AL_RHST) sites, denoted with black (blue) hollow circle in Figure 7a. The period for validation based on the CALM (AL_RHST) data is 1991–2000 (1981–1990).

to 3.23 m (CFSR simulation), from 0 to 7.92 m (ERA-I simulation), and from 0 to 3.02 m (MERRA simulation), with area-averaged values of 1.10 m (CFSR simulation), 1.13 m (ERA-I simulation), and 1.26 m (MERRA simulation). The CALM observation-based validation shows that the simulated active layer thickness is significantly correlated to the observations and has a positive mean bias ranging from 0.21 m (CFSR simulation) to 0.66 m (MERRA simulation). When AL_RHST observations are used for validation, the correlation between simulations and observations weakens, and a negative bias is present, with a range from -0.11 m (MERRA simulation) to -0.33 m (CFSR simulation). Such positive (based on CALM observations) and negative biases (based on AL_RHST observations) in active layer thickness are related to warm (based on IPY-TSP observations) and cold (based on RMS observations) biases in the soil temperature. Among the three simulations, the CFSR and ERA-I simulations generally show a more reasonable active layer thickness than the MERRA simulation (Table 2).

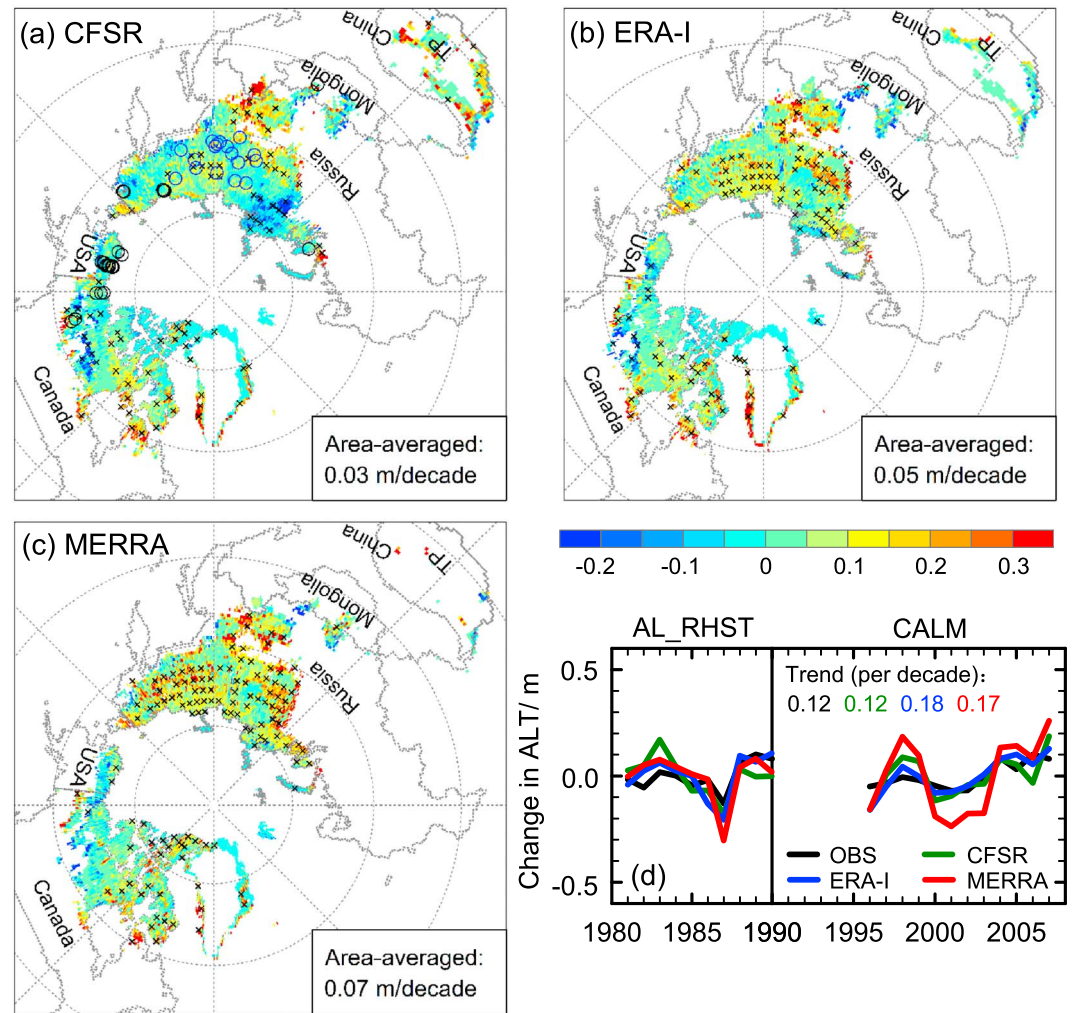


Figure 8. Similar as in Figure 3 but for simulated active layer thickness (ALT) trends (m decade^{-1}) from 1979 to 2009 over the simulated permafrost region where permafrost remains in each year during the period 1979–2009. In addition, in Figure 8d, the validation for the period 1981–1990 (1996–2007) is based on observations from AL_RHST (CALM).

Compared to the spatial distribution of trends in soil temperature and permafrost extent, the three simulations produce more inconsistencies in the spatial distribution of trends in the active layer thickness (Figure 8). For example, the CFSR-based simulation shows a negative center in the Northern Siberian Plain, Russia, which is not present in the results from the ERA-I and MERRA simulations. The CFSR and ERA-I simulations show negative trends in the Canadian Archipelago, whereas the MERRA simulation shows a positive trend. In spite of these differences, all three simulations produce positive trends in the active layer thickness in the hinterlands of Russia and Canada, as well as negative trends at the grids situated at the southern edge of the high-latitude permafrost region (such as the southern edge of the permafrost in Alaska and the edge of permafrost in Sayan and on mountains in south Baikal). Observations-based validation shows that the CFSR- and ERA-I-based simulations capture the interannual variations in active layer thickness reasonably, but the MERRA-based simulation distinctly magnifies the amplitude of the variations. The trend from the CFSR simulation ($0.12 \text{ m decade}^{-1}$) is the same as the observations of $0.12 \text{ m decade}^{-1}$, while trends from the ERA-I ($0.18 \text{ m decade}^{-1}$) and MERRA ($0.17 \text{ m decade}^{-1}$) simulations are close to but higher than the observations.

The active layer thickness experiences a significant increase from 1979 to 2009, as indicated by all three simulations (Figure 9). The area-averaged trends in active layer thickness are 0.03 , 0.05 , and $0.07 \text{ m decade}^{-1}$ for the CFSR, ERA-I, and MERRA simulations, respectively. The average trend is $0.05 \text{ m decade}^{-1}$, with one standard deviation of $0.016 \text{ m decade}^{-1}$ across the three simulations (Table 3). The relative change in active layer

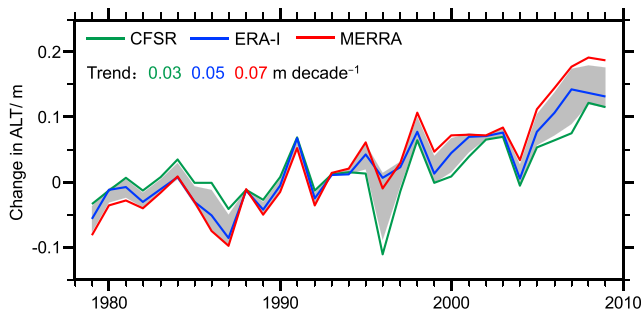


Figure 9. Simulated change in active layer thickness (ALT) (m) based on atmospheric forcing data sets from CFSR, ERA-I, and MERRA from 1979 to 2009, as averaged over the simulated permafrost region where permafrost remains in each year during the period 1979–2009. Shaded areas represent one standard deviation across the simulations based on the three types of atmospheric forcing data sets. The simulated trends are given in the top left corner of the figure.

thickness is 9.9%, 16.0%, and 20.2% for the CFSR-, ERA-I-, and MERRA-based simulations, respectively, indicating a considerable range resulting from the different atmospheric forcing data sets.

4. Discussions

Soil temperature observations at depths of 1 m from (RMS) and 6 m (IPY-TSP) as well as the active layer thickness from two sources (CALM and AL_RHST), were collected to validate both simulated present-day climatology and recent variations in permafrost-related variables. The results show that the three simulations can reproduce the recent variations in soil temperature and active layer thickness. For present-day climatology, however, the simulations produce a 1.82–1.99°C cold bias in soil temperature at 1 m depth. The same cold bias was also found in the simulated results by CLM4.0 (Lawrence et al., 2012). Lawrence et al. (2012) explained that the cold bias may be a result of excessively dry simulated soil in the active layer of organic-rich regions. Dry soils have lower thermal conductivity, which limits heat penetration into the soil during the

summer. This results in lower soil temperature with associated shallow active layer. Cold-region hydrology has been updated in CLM4.5, including the hydraulic properties of frozen ground that is modified to depend on liquid content rather than total water content, incorporation of an ice impedance function, and correction of the consistency between soil water state and water table position (Swenson et al., 2012). However, the cold bias in soil temperature can still be seen in CLM4.5 in the results presented here. Further research and model development are thus required to correct for these cold biases. Despite the cold bias in the 1 m soil temperature, a smaller and positive bias (0.22–1.16°C) is shown in the deeper soil layer at 6 m. This indicates that CLM4.5 may be better at capturing the soil temperature at deeper layers. The same conclusion is reached by Guo and Yang (2010) using the Simultaneous Heat and Water model (Guo & Yang, 2010).

It should be mentioned that scale mismatch in this comparison may contribute to the bias in soil temperature and active layer thickness. Our comparisons are based on individual site observations and the corresponding grid mean simulated results. In regions with varied topography, soil temperature and active layer thickness tend to vary substantially over small distances (Lawrence et al., 2012). In this case, a grid mean value might not be accurately represented by site observations contained within the grid. This mismatch in scale was also encountered and explained by Lawrence et al. (2012). However, the horizontal resolution used in the present work is about twice that ($0.94^\circ \times 1.25^\circ$) used in Lawrence et al. (2012), which would be expected to weaken the impact of the scale mismatch.

This study produces a smaller simulated permafrost area than the circum-Arctic map of permafrost and ground ice conditions (Brown et al., 1997). This mostly happened over the Tibetan Plateau region, where the simulated permafrost extent is considerably smaller than in the observations. The simulated permafrost area refers to “near-surface” permafrost, which is of more concern due to its greater sensitivity to climate change. The circum-Arctic map of permafrost and ground ice conditions does not distinguish between near-surface and deeper permafrost. When a deeper soil layer standard (upper 11 soil layers (6.3 m)) is included in permafrost identification, the permafrost extent in high latitudes shows a slight increase, whereas the permafrost extent over the Tibetan Plateau shows a larger increase (not shown). The active layer thickness (permafrost table) is shallow for high-latitude permafrost but relatively deep for the high-elevation permafrost over the Tibetan Plateau. Consequently, when using the shallow layer standard to identify permafrost, high-latitude permafrost is identified but the high-elevation permafrost over the Tibetan Plateau is not. This implies that different standards should be used to identify high-latitude and high-elevation permafrost in the future.

Nevertheless, the simulated permafrost extent over the Tibetan Plateau is still much smaller than that derived from observations, even if a standard of the upper 12 soil layers (10.4 m) is used to identify permafrost (not shown). When a suite of new, high-resolution atmospheric forcing data set (HY data) were used to drive CLM4.0, a reasonable permafrost extent was obtained on the Tibetan Plateau (Guo & Wang, 2013). As an update from CLM4.0, CLM4.5 (as used in this study) is less prone to this bias. Consequently, the

Table 4
Relative Sensitivity of Simulated Permafrost Extent to Different Factors, Including Model Physics and Atmospheric Forcing Data Sets

	CLM3.5 (revised hydrology)	Organic soil	Organic soil +50 m deep soil column	Simulated climate bias	Different forcing data sets
Relative sensitivity	−3.6%	+14.4%	+15.8%	−7.9%	+6.1% (MERRA to ERA-I); +14.9% (MERRA to CFSR)
Reference	Lawrence et al. (2008)	Lawrence et al. (2008)	Lawrence et al. (2008)	Lawrence et al. (2012)	This Study

Note. Observed permafrost areas used to calculate relative sensitivity are $15.2 \times 10^6 \text{ km}^2$ (the Northern Hemisphere) and $13.9 \times 10^6 \text{ km}^2$ (north of 45°N) from the circum-Arctic map of permafrost and ground ice conditions (Brown et al., 1997). Relative sensitivity is calculated as (simulated permafrost area − observations)/observations $\times 100\%$. Negative symbol means that the sensitivity is away from observations, whereas positive symbol means that the sensitivity is close to observations.

atmospheric forcing data sets developed from reanalysis data are likely to be responsible for the bias. This suggests that the reanalysis-based atmospheric forcing data set may be less suitable for the simulation of permafrost over the Tibetan Plateau based on CLM.

The smallest increase in simulated annual soil temperature at 1 m depth is seen in the CFSR-based simulation ($0.46^\circ\text{C decade}^{-1}$), followed by the ERA-I-based ($0.60^\circ\text{C decade}^{-1}$) and MERRA-based ($0.60^\circ\text{C decade}^{-1}$) simulations. As shown in Table 1, the smallest increase in annual air temperature is seen in the CFSR-based ($0.44^\circ\text{C decade}^{-1}$) and MERRA-based simulation ($0.44^\circ\text{C decade}^{-1}$), followed by the ERA-I-based simulation ($0.50^\circ\text{C decade}^{-1}$). While the MERRA-based simulation shows the lowest increase in annual air temperature, this is not consistent with the same simulation showing the greatest increase in soil temperature (Table 1). This inconsistency may be caused by snow depth. The MERRA-based simulation has the shallowest snow depth among the three simulations (Table 1). Less snow means there is less of an insulating effect, making it easier for heat from air temperature increase to penetrate into the soil, resulting in higher soil temperature.

The smallest decreases in simulated permafrost area are seen in the ERA-I-based simulation ($-0.28 \times 10^6 \text{ km}^2 \text{ decade}^{-1}$), followed by the MERRA-based ($-0.29 \times 10^6 \text{ km}^2 \text{ decade}^{-1}$) and CFSR-based ($-0.36 \times 10^6 \text{ km}^2 \text{ decade}^{-1}$) simulations. While the CFSR-based simulation shows the most decrease in permafrost area, this is not consistent with the same simulation showing the smallest increase in soil temperature ($0.46^\circ\text{C decade}^{-1}$) at 1 m depth. This inconsistency is because CFSR-based simulation produces distinctly more permafrost on the Tibetan Plateau than ERA-I- and MERRA-based simulations and the permafrost on the Tibetan Plateau shows apparent decrease in area (Figures 6a–6c), which results in the most decrease in total permafrost area in CFSR-based simulation. When permafrost change on the Tibetan Plateau is not taken into account, the smallest decreases in simulated permafrost area are seen in the CFSR-based simulation ($-0.19 \times 10^6 \text{ km}^2 \text{ decade}^{-1}$), followed by the ERA-I-based ($-0.25 \times 10^6 \text{ km}^2 \text{ decade}^{-1}$) and MERRA-based ($-0.28 \times 10^6 \text{ km}^2 \text{ decade}^{-1}$) simulations. This order is consistent with that of the increase in simulated soil temperature.

The smallest increases in active layer thickness are seen in the CFSR-based simulation ($0.03 \text{ m decade}^{-1}$), followed by the ERA-I-based ($0.05 \text{ m decade}^{-1}$) and MERRA-based ($0.07 \text{ m decade}^{-1}$) simulations. This order is consistent with that of the increase in simulated soil temperature. In spite of the relation with soil temperature, changes in permafrost area and active layer thickness are related to the present-day climatology of soil temperature. This is because the changes in permafrost area and active layer thickness are identified according to whether or not the soil temperature is above 0°C . Colder permafrost is less likely to reach 0°C than warmer permafrost and thus has a smaller rate of change, if the same increase in soil temperature is assumed to occur. Indeed, differences in permafrost area—and active layer thickness—change among the three simulations correspond favorably to their present-day climatology of soil temperature (Table 1).

In order to examine the relative importance of atmospheric forcing data sets with other factors such as model physics to permafrost simulation, we compare the percentage sensitivities of permafrost simulation to different atmospheric forcing data sets and model physics improvements. It is found that the sensitivity (+14.9%) of changing MERRA to CFSR is close to those of organic soil (+14.4%) and organic soil +50 m deep soil column

(+15.8%) (Table 4). This indicates that different atmospheric forcing data sets could be of the same importance as improvements of some model physics.

5. Conclusion

Sensitivities in the simulation of permafrost to different atmospheric forcing data sets were investigated in this study. The reanalysis-based simulation makes a more reasonable estimate of the recent interannual variations than the climatology in soil temperature and active layer thickness. The CFSR- and ERA-I-based simulations overall produce better estimates of permafrost extent and active layer thickness than the MERRA-based simulation. The three simulations produce similar spatial patterns of present-day climatology and trends in soil temperature and permafrost extent, except over the Tibetan Plateau. However, the ranges seen in the simulated temporal changes in area-averaged permafrost area (−5.8% to −9.0%) and active layer thickness (9.9%–20.2%), indicate that different atmospheric forcing data sets are responsible for uncertainties in the results of permafrost simulation.

These results are useful for understanding the impacts of atmospheric forcing data set on permafrost simulation. The differences in the results for permafrost change among the three simulations are mostly related to the differences in air temperature increase, snow depth, and permafrost temperature conditions in these simulations. Previous studies on the improvement of permafrost simulations concentrated mainly on the modifications of the frozen-ground process of the model (Lawrence et al., 2008, 2011). The present study focuses on the impacts of different atmospheric forcing data sets on the simulated permafrost results. In the present study, cold biases of 1.82–1.99°C are still found in the soil temperature at 1 m depth simulated by CLM4.5, despite the model's update with respect to hydraulic properties in cold regions. Further research and model development are underway to correct these cold biases in the future.

Acknowledgments

This research was jointly supported by the National Natural Science Foundation of China (41405087 and 41775076), the National Key Research and Development Program of China (grant 2016YFA0600704), and the External Cooperation Program of BIC, Chinese Academy of Sciences (134111KYSB20150016). We wish to thank: the European Centre for Medium-Range Weather Forecasts (ECMWF) for providing the ERA-I reanalysis data (<http://apps.ecmwf.int/datasets/data/interim-full-mode/levtype=sfc/>); the Modeling and Assimilation Data and Information Services Center (MDISC), managed by the NASA Goddard Earth Sciences (GES) Data and Information Services Center (DISC) for providing the MERRA data (<https://gmao.gsfc.nasa.gov/reanalysis/MERRA/>); the CISM Research Data Archive managed by NCAR's Data Support Section Data for Atmospheric and Geosciences Research for providing the CFSR data (<https://rda.ucar.edu/>); and the National Snow and Ice data Center (NSIDC) for providing the circum-Arctic map of permafrost and ground ice conditions (http://nsidc.org/data/docs/fgdc/ggd318_map_circumarctic/index.html).

References

- Alexeev, V. A., Nicolsky, D. J., Romanovsky, V. E., & Lawrence, D. M. (2007). An evaluation of deep soil configurations in the CLM3 for improved representation of permafrost. *Geophysical Research Letters*, 34(9), L09502. <https://doi.org/10.1029/2007GL029536>
- Bosilovich, M. G., Robertson, F. R., & Chen, J. (2011). Global energy and water budgets in MERRA. *Journal of Climate*, 24(22), 5721–5739. <https://doi.org/10.1175/2011JCLI4175.1>
- Brown, J., Ferrians, O. J. Jr, Heginbottom, J. A., & Melnikov, E. S. (1997). Circum-Arctic map of permafrost and ground-ice conditions. U.S. Geol. Surv. in Cooperation with the Circum-Pacific Council for Energy and Mineral Resources, Circum-Pacific Map Series CP-45, scale 1:10,000,000, 1 sheet.
- Brown, J., Hinkel, K., & Nelson, F. (2000). The Circumpolar Active Layer Monitoring (CALM) program: Research designs and initial results. *Polar Geography*, 24, 165–258.
- Burn, C. R., & Nelson, F. E. (2006). Comment on "A projection of severe near-surface permafrost degradation during the 21st century" by David M. Lawrence and Andrew G. Slater. *Geophysical Research Letters*, 33(21), L21503. <https://doi.org/10.1029/2006GL027077>
- Chen, H. S., Teng, F., Zhang, W., & Liao, H. (2017). Impacts of anomalous mid-latitude cyclone activity over East Asia during summer on the decadal mode of East Asian summer monsoon and its possible mechanism. *Journal of Climate*, 30(2), 739–753. <https://doi.org/10.1175/JCLI-D-16-0155.1>
- Collins, M., Knutti, R., Arblaster, J., Dufresne, J.-L., Fichefet, T., Friedlingstein, P., ... Gutowski, W. J. (2013). Long-term climate change: Projections, commitments and irreversibility. In T. F. Stocker, et al. (Eds.), *Climate change 2013: The Physical Science Basis. Contribution of Working Group I to the Fifth Assessment Report of the Intergovernmental Panel on Climate Change*, (pp. 1029–1136). Cambridge, UK, and New York: Cambridge Univ. Press.
- Cuo, L., Zhang, Y., Bohn, T. J., Zhao, L., Li, J., Liu, Q., & Zhou, B. (2015). Frozen soil degradation and its effects on surface hydrology in the northern Tibetan Plateau. *Journal of Geophysical Research: Atmospheres*, 120(16), 8276–8298. <https://doi.org/10.1002/2015JD023193>
- Dee, D., Uppala, S., Simmons, A., Berrisford, P., Poli, P., Kobayashi, S., ... Balsaseda, M. A. (2011). The ERA-Interim reanalysis: Configuration and performance of the data assimilation system. *Quarterly Journal of the Royal Meteorological Society*, 137(656), 553–597. <https://doi.org/10.1002/qj.828>
- Fan, K., Xie, Z., & Xu, Z. (2016). Two different periods of high dust weather frequency in northern China. *Atmospheric and Oceanic Science Letters*, 9(4), 263–269. <https://doi.org/10.1080/16742834.2016.1176300>
- Flanner, M. G., Zender, C. S., Randerson, J. T., & Rasch, P. J. (2007). Present day climate forcing and response from black carbon in snow. *Journal of Geophysical Research*, 112(D11), D11202. <https://doi.org/10.1029/2006JD008003>
- Gao, X. J., Shi, Y., & Giorgi, F. (2016). Comparison of convective parameterizations in RegCM4 experiments over China with CLM as the land surface model. *Atmospheric and Oceanic Science Letters*, 9(4), 246–254. <https://doi.org/10.1080/16742834.2016.1172938>
- Guo, D. L., & Sun, J. Q. (2015). Permafrost thaw and associated settlement hazard onset timing over the Qinghai-Tibet engineering corridor. *International Journal of Disaster Risk Science*, 6(4), 347–358. <https://doi.org/10.1007/s13753-015-0072-3>
- Guo, D. L., & Wang, H. J. (2013). Simulation of permafrost and seasonally frozen ground conditions on the Tibetan Plateau, 1981–2010. *Journal of Geophysical Research: Atmospheres*, 118(11), 5216–5230. <https://doi.org/10.1002/jgrd.50457>
- Guo, D. L., & Wang, H. J. (2016a). Permafrost degradation and associated ground settlement estimation under 2°C global warming. *Climate Dynamics*, 49(7–8), 2569–2583. <https://doi.org/10.1007/s00382-016-3469-9>
- Guo, D. L., & Wang, H. J. (2016b). CMIP5 permafrost degradation projection: A comparison among different regions. *Journal of Geophysical Research: Atmospheres*, 121(9), 4499–4517. <https://doi.org/10.1002/2015JD024108>

- Guo, D. L., Wang, H. J., & Li, D. (2012). A projection of permafrost degradation on the Tibetan Plateau during the 21st century. *Journal of Geophysical Research*, 117(D5), D05106. <https://doi.org/10.1029/2011JD016545>
- Guo, D. L., & Yang, M. X. (2010). Simulation of soil temperature and moisture in seasonally frozen ground of central Tibetan Plateau by SHAW model [in Chinese]. *Plateau Meteorology*, 29, 1369–1377.
- Huffman, G. J., Adler, R. F., Bolvin, D. T., & Gu, G. (2009). Improving the global precipitation record: GPCP version 2.1. *Geophysical Research Letters*, 36(17), L17808. <https://doi.org/10.1029/2009GL040000>
- Koven, C. D., Riley, W. J., & Stern, A. (2013). Analysis of permafrost thermal dynamics and response to climate change in the CMIP5 Earth system models. *Journal of Climate*, 26(6), 1877–1900. <https://doi.org/10.1175/JCLI-D-12-00228.1>
- Lawrence, P. J., & Chase, T. N. (2007). Representing a MODIS consistent land surface in the Community Land Model (CLM 3.0). *Journal of Geophysical Research*, 112(G1), G01023. <https://doi.org/10.1029/2006JG000168>
- Lawrence, D. M., Oleson, K. W., Flanner, M. G., Thornton, P. E., Swenson, S. C., Lawrence, P. J., ... Slater, A. G. (2011). Parameterization improvements and functional and structural advances in version 4 of the Community Land Model. *Journal of Advances in Modeling Earth Systems*, 3(3), M03001. <https://doi.org/10.1029/2011MS000045>
- Lawrence, D. M., & Slater, A. G. (2005). A projection of severe nearsurface permafrost degradation during the 21st century. *Geophysical Research Letters*, 32(24), L24401. <https://doi.org/10.1029/2005GL025080>
- Lawrence, D. M., Slater, A. G., Romanovsky, V. E., & Nicolsky, D. J. (2008). Sensitivity of a model projection of near-surface permafrost degradation to soil column depth and representation of soil organic matter. *Journal of Geophysical Research*, 113(F2), F02011. <https://doi.org/10.1029/2007JF000883>
- Lawrence, D. M., Slater, A. G., & Swenson, S. C. (2012). Simulation of present-day and future permafrost and seasonally frozen ground conditions in CCSM4. *Journal of Climate*, 25(7), 2207–2225. <https://doi.org/10.1175/JCLI-D-11-00334.1>
- Liljedahl, A. K., Boike, J., Daanen, R. P., Fedorov, A. N., Frost, G. V., Grosse, G., ... Zona, D. (2016). Pan-Arctic ice-wedge degradation in warming permafrost and its influence on tundra hydrology. *Nature Geoscience*, 9(4), 312–318. <https://doi.org/10.1038/ngeo2674>
- Liu, Y., & Jiang, D. (2016). Mid-Holocene permafrost: Results from CMIP5 simulations. *Journal of Geophysical Research: Atmospheres*, 121, 221–240.
- Muller, S. W. (1947). *Permafrost or permanently frozen ground and related engineering problems*, (p. 231). Ann Arbor: J. W. Edwards.
- Nash, J. E., & Sutcliffe, J. V. (1970). River flow forecasting through conceptual models. Part I: A discussion of principles. *Journal of Hydrology*, 10(3), 282–290. [https://doi.org/10.1016/0022-1694\(70\)90255-6](https://doi.org/10.1016/0022-1694(70)90255-6)
- Nelson, F. E., Anisimov, O. A., & Shiklomanov, N. (2002). Climate change and hazard zonation in the circum-Arctic permafrost regions. *Natural Hazards*, 26(3), 203–225. <https://doi.org/10.1023/A:1015612918401>
- Nicolsky, D. J., Romanovsky, V. E., Alexeev, V. A., & Lawrence, D. M. (2007). Improved modeling of permafrost dynamics in a GCM land-surface scheme. *Geophysical Research Letters*, 34(8), L08501. <https://doi.org/10.1029/2007GL029525>
- Niu, G. Y., & Yang, Z. L. (2006). Effects of frozen soil on snowmelt runoff and soil water storage at a continental scale. *Journal of Hydrometeorology*, 7(5), 937–952. <https://doi.org/10.1175/JHM538.1>
- Niu, G. Y., Yang, Z. L., Dickinson, R. E., Gulden, L. E., & Su, H. (2007). Development of a simple groundwater model for use in climate models and evaluation with Gravity Recovery and Climate Experiment data. *Journal of Geophysical Research*, 112(D7), D07103. <https://doi.org/10.1029/2006JD007522>
- Oleson, K., Bonan, G. B., Drewniak, B., Huang, M., Koven, C. D., Levis, S., ... Riley, W. J. (2013). Technical description of version 4.5 of the Community Land Model (CLM). NCAR Tech. Note NCAR/TN-503+STR, 434 pp., National Center for Atmospheric Research, Boulder, CO.
- Qin, D. H., Zhou, B. T., & Xiao, C. D. (2014). Progress in studies of cryospheric changes and their impacts on climate of China. *Journal of Meteorological Research*, 28(5), 732–746. <https://doi.org/10.1007/s13351-014-4029-z>
- Rienecker, M. M., Suarez, M. J., Gelaro, R., Todling, R., Bacmeister, J., Liu, E., ... Schubert, S. D. (2011). MERRA: NASA's Modern-Era Retrospective Analysis for Research and Applications. *Journal of Climate*, 24(14), 3624–3648. <https://doi.org/10.1175/JCLI-D-11-00015.1>
- Romanovsky, V. E., Smith, S. L., & Christiansen, H. H. (2010). Permafrost thermal state in the polar Northern Hemisphere during the international polar year 2007–2009: A synthesis. *Permafrost and Periglacial Processes*, 21(2), 106–116. <https://doi.org/10.1002/ppp.689>
- Saha, S., Moorthi, S., Pan, H.-L., Wu, X., Wang, J., Nadiga, S., ... Kistler, R. (2010). The NCEP climate forecast system reanalysis. *Bulletin of the American Meteorological Society*, 91(8), 1015–1058. <https://doi.org/10.1175/2010BAMS3001.1>
- Schuur, E., McGuire, A. D., Schädel, C., Grosse, G., Harden, J. W., Hayes, D. J., ... Vonk, J. E. (2015). Climate change and the permafrost carbon feedback. *Nature*, 520(7546), 171–179. <https://doi.org/10.1038/nature14338>
- Sun, B. (2017). Seasonal evolution of the dominant modes of the Eurasian snowpack and atmospheric circulation from autumn to the subsequent spring and the associated surface heat budget. *Atmospheric and Oceanic Science Letters*, 10(3), 191–197. <https://doi.org/10.1080/16742834.2017.1286226>
- Swenson, S. C., Lawrence, D. M., & Lee, H. (2012). Improved simulation of the terrestrial hydrological cycle in permafrost regions by the Community Land Model. *Journal of Advances in Modeling Earth Systems*, 4(3), M08002. <https://doi.org/10.1029/2012MS000165>
- Thornton, P. E., Doney, S. C., Lindsay, K., Moore, J. K., Mahowald, N., Randerson, J. T., ... Lee, Y. H. (2009). Carbon-nitrogen interactions regulate climate-carbon cycle feedbacks: Results from an atmosphere-ocean general circulation model. *Biogeosciences*, 6(10), 2099–2120. <https://doi.org/10.5194/bg-6-2099-2009>
- Thornton, P. E., & Zimmermann, N. E. (2007). An improved canopy integration scheme for a land surface model with prognostic canopy structure. *Journal of Climate*, 20(15), 3902–3923. <https://doi.org/10.1175/JCLI4222.1>
- Wang, Y., Xie, Z., Jia, B., & Yu, Y. (2015). Improving simulation of the terrestrial carbon cycle of China in version 4.5 of the Community Land Model using a revised Vcmax scheme. *Atmospheric and Oceanic Science Letters*, 8, 88–94.
- Wang, A. H., & Zeng, X. B. (2009). Improving the treatment of vertical snow burial fraction over short vegetation in the NCAR CLM3. *Advances in Atmospheric Sciences*, 26(5), 877–886. <https://doi.org/10.1007/s00376-009-8098-3>
- Wang, A. H., & Zeng, X. B. (2012). Evaluation of multireanalysis products with in situ observations over the Tibetan Plateau. *Journal of Geophysical Research: Atmospheres*, 117(D5), D05102. <https://doi.org/10.1029/2011JD016553>
- Wang, A. H., Zeng, X. B., & Guo, D. L. (2016). Estimates of global surface hydrology and heat fluxes from the Community Land Model (CLM4.5) with four atmospheric forcing datasets. *Journal of Hydrometeorology*, 17(9), 2493–2510. <https://doi.org/10.1175/JHM-D-16-0041.1>
- Xie, Z. H., Wang, L., Jia, B., & Yuan, X. (2016). Measuring and modeling the impact of a severe drought on terrestrial ecosystem CO₂ and water fluxes in a subtropical forest. *Journal of Geophysical Research: Biogeosciences*, 121, 2576–2587.
- Yang, M. X., Nelson, F., Shiklomanov, N., Guo, D. L., & Wan, G. (2010). Permafrost degradation and its environmental effects on the Tibetan Plateau: A review of recent research. *Earth Science Reviews*, 103(1–2), 31–44. <https://doi.org/10.1016/j.earscirev.2010.07.002>
- Yang, K., Wu, H., Qin, J., Lin, C., Tang, W., & Chen, Y. (2014). Recent climate changes over the Tibetan Plateau and their impacts on energy and water cycle: A review. *Global and Planetary Change*, 112, 79–91. <https://doi.org/10.1016/j.gloplacha.2013.12.001>

- Yi, S., Wang, X., Qin, Y., Xiang, B., & Ding, Y. (2014). Responses of alpine grassland on Qinghai-Tibetan Plateau to climate warming and permafrost degradation: A modeling perspective. *Environmental Research Letters*, 9(7), 074014. <https://doi.org/10.1088/1748-9326/9/7/074014>
- Zhang, T., Barry, R. G., Knowles, K., Heginbottom, J. A., & Brown, J. (1999). Statistics and characteristic of permafrost and ground-ice distribution in the Northern Hemisphere. *Polar Geography*, 23(2), 132–154. <https://doi.org/10.1080/10889379909377670>
- Zhang, T., Frauenfeld, O. W., & Barry, R. G. (2006). Time series of active layer thickness in the Russian Arctic, 1930–1990, National Snow and Ice Data Center, Boulder (digital media).
- Zhou, B. T., Xu, Y., Wu, J., Dong, S., & Shi, Y. (2016). Changes in temperature and precipitation extreme indices over China: Analysis of a high-resolution grid dataset. *International Journal of Climatology*, 36(3), 1051–1066. <https://doi.org/10.1002/joc.4400>

UNCORRECTED PROOF